Chapter 4

Bond disorder enhances the information transfer in the polar flock

4.1 Introduction

In the previous chapter.3, we have studied the effect of bond disorder on the ordered flock, where we find that bond disorder does not effect the usual long range ordering and enhances the cohesion among the polar flock. Further, the ordering kinetics and usual giant number fluctuation remain unaffected. In this chapter, we discuss the effect of bond disorder on SPPs near to the order-disorder transition. Recently, there is a growing interest in understanding the effects and advantages of different kinds of inhomogeneity that are omnipresent in nature. Many studies show that inhomogeneity can destroy the LRO present in a clean system [Chepizhko et al. (2013); Das et al. (2018); Morin et al. (2017); Quint & Gopinathan (2015); Reichhardt & Reichhardt (2017); Sándor et al. (2017); Toner et al. (2018a,b); Yllanes et al. (2017)], whereas a few studies discuss special kinds of inhomogeneity that enhance the ordering in the system [Das et al. (2020); Pattanayak et al. (2020)]. Therefore inhomogeneity can be useful for many practical applications, e.g., crowd control and faster evacuation, etc. [Beatrici et al. (2017); Bhattacherjee et al. (2015);

Bishop & Reppy (1978); Bray (1994); Frank & Dorso (2011); Garcimartín et al. (2018); Kumar & Mishra (2020); Kumar et al. (2017, 2021); Pattanayak et al. (2021); Singh & Mishra (2020); Wittkowski et al. (2014); Zuriguel et al. (2011, 2016)].

In the Vicsek model, each individual interacts through a short-range alignment interaction, and the strength of the interaction is the same for all the particles. But in natural systems, each particle can have a different ability to influence its neighbours based on their individual intelligence or physical strength, etc. However, scientists have not paid much attention to understand the effects of different interaction strengths in a polar flock. In a recent study, Bialek *et al.* [Bialek et al. (2012)] show that the varying interaction strength of the SPPs results in maximum entropy. Hence, more information transfer among the particles [Bialek et al. (2012)][Pattanayak et al. (2020)]. Surprisingly, in this work, we note that the presence of inhomogeneity in the form of the particles' different interaction ability, the system approaches towards a more homogeneous state near to the point of order-disorder transition. More importantly, the flock's response is faster for higher disorder in the interaction strength among the SPPs because each SPP neighbour is updated more frequently, which leads to faster information transfer within the flock. We also calculate the systems' information entropy [Ben-Naim (2015); Cavagna et al. (2014); Pritišanac et al. (2019); Shannon (1948)] for different disorders and find that the larger the disorder, the more is the systems' information entropy.

Further, we have characterised the effect of bond disorder on the nature of disorder-to-order phase transition in the system. The nature of phase transition in an active system has been a matter of great interest in many previous studies [Ben-Naim (2015); Nagy et al. (2007); Pattanayak & Mishra (2018); Singh et al. (2021)]. The effect of random impurities shows interesting results in many equilibrium systems [Janoschek et al. (2013); Korshunov (1992); Maucourt & Grempel (1997); Shastry (1982)] as well. In the study, M. Durve *et al.* [Durve & Sayeed (2016)] have found a first-order phase transition by tuning particles' view

angle in the modified Vicsek model. However, the results observed for phase transitions are very much model-dependent. Our numerical simulation suggests that the nature of the disorder-to-order phase transition changes from discontinuous to continuous type by tuning the strength of bond disorder. Also, the system shows the enhanced ordering near the transition point for the larger disorder.

The rest of the chapter is organized as follows. In Sec.4.2 , we discuss the model and simulation details. In Sec.4.3 , the results from the numerical simulations are discussed. In Sec.4.4 , we conclude the chapter with a summary and discussion on the obtained results.

4.2 Model

We consider a collection of N number of polar self-propelled particles (SPPs) moving on a two-dimensional substrate. SPPs interact through a short-range alignment interaction within a small interaction radius R_I [Ben-Naim (2015); Grégoire & Chaté (2004); Vicsek et al. (1995)]. Moreover, the strength of interaction of each SPP with its neighbours is *different*, unlike the Vicsek model [Vicsek et al. (1995)] of uniform interaction strength. Each SPP is defined by its position $\mathbf{r}_i(t)$ with orientation $\theta_i(t)$, and it moves along its direction vector $\mathbf{n}_i(t) = \big(\cos(\theta_i(t)), \sin(\theta_i(t))\big)$ with a fixed speed v_0. The two update equations for the position $\mathbf{r}_i(t)$ and the direction vector $\mathbf{n}_i(t)$ are given by,

$$\mathbf{r}_i(t+\Delta t) = \mathbf{r}_i(t) + v_0 \mathbf{n}_i(t)\Delta t \tag{4.1}$$

$$\mathbf{n}_i(t+\Delta t) = \frac{\sum_{j\in R_I} J_j \mathbf{n}_j(t) + \eta N_i(t)\mathbf{k}_i(t)}{w_i(t)} \tag{4.2}$$

The first equation represents the particle's motion due to its self-propelled nature along the direction vector $\mathbf{n}_i(t)$ with fixed speed v_0. $\Delta t = 1.0$ is the unit time step. The first term in Eq ∼(4.2) represents the short-range alignment interaction of the i^{th} particle with its

neighbours within the interaction radius (R_I), and J_j is the interaction strength of the j^{th} neighbour. The probability distribution of the interaction strength J, $P(J)$ is obtained from a uniform distribution of range $[1-\frac{\varepsilon}{2} : 1+\frac{\varepsilon}{2}]$ [Kumar et al. (2017)], where ε measures the degree of disorder. $\varepsilon = 0$ corresponds to the uniform interaction strength ($J_i = 1$, for all the particles) like the Vicsek model [Vicsek et al. (1995)], whereas $\varepsilon = 2$ corresponds to the maximum disorder in the system. Furthermore, the second term in Eq ∼(4.2) denotes the vector noise, which measures the particle's error while following its neighbours. $\mathbf{k}_i(t)$ is a random unit vector where $N_i(t)$ denotes the number of neighbours within the interaction radius of the i^{th} particle at time t. η represents the strength of the noise and can vary from 0.0 to 1.0. $w_i(t)$ is the normalization factor, which reduces the right-hand side of the Eq ∼(4.2) to a unit vector.

For zero self-propulsion speed, the model reduces to the *equilibrium* random bond XY-model [Dieny & Barbara (1990); Kumar et al. (2017)]. However, for $\varepsilon = 0$, the model reduces to the *clean* polar flock. We numerically update the Eqs ∼(4.1) and (4.2) for all SPPs sequentially. One simulation step is counted after the update of Eqs ∼(4.1) and (4.2) once for all the particles. Periodic boundary condition (PBC) is used for the system. All the lengths are measured in terms of interaction radius $R_I = 1.0$. The size of the system L is varied from 90 to 200. Here system size L means L times the interaction radius. The number density of the system is defined as $\rho_N = \frac{N}{L\times L}$. We fix the density at $\rho_N = 1.0$ and self-propulsion speed $v_0 = 0.5$. Since for the same density for the clean polar flock, the critical noise is close to $\eta \sim 0.6$. Hence, we limit our study near the critical point, and the noise strength is varied from $\eta = 0.4$ - 0.8 to study the phase transition, and keeping fixed $\eta = 0.62$ to characterise the properties of polar flock near to critical point. We considered time up to 10^6 simulation steps and 20 independent realisations for different values of disorder strength ε. Although the time is taken to reach the steady state depends on the

disorder strength, but for all disorders, steady-state is obtained by 10^4 simulation steps, and the remaining time is used for time averaging.

4.3 Results

4.3.1 Disorder-to-order transition

First, we study the disorder-to-order transition in the system for different disorder strengths ε. Ordering in the system is characterised by the mean orientation order parameter,

$$\psi(t) = \frac{1}{N}|\sum_{i=1}^{N} n_i(t)| \tag{4.3}$$

In the ordered state, i.e., when most particles are moving in the same direction, then ψ will be closer to 1.0 and of the order of $\frac{1}{\sqrt{N}}$ for a random disordered state. In Fig.4.1(a), we have shown the variation of $\psi(t)$ with the noise strength η for three different $\varepsilon = (0,$ 1 and 2). For $\varepsilon = 0$, the variation of ψ shows a sharp change from $\psi \sim 1.0$ to ~ 0.0. This kind of change is a common feature of first-order phase transition [Ben-Naim (2015); Bricard et al. (2013); Chaté et al. (2008); Chepizhko et al. (2013); Pattanayak & Mishra (2018)]. Whereas for $\varepsilon = 2$, ψ varies continuously, and the transition has a signature of second-order phase transition. The variation of ψ for $\varepsilon = 1$ shows the intermediate behaviour. The plot of order parameter fluctuation or the susceptibility $\xi = \sqrt{< \psi^2 > - < \psi >^2}$ is shown in Fig.4.1(b) where $< ... >$ denotes the average over steady-state time. The critical noise η_c is obtained from the maximum of ξ. The $\eta_c(\varepsilon)$ shifts towards the right on increasing $\varepsilon = 0,$ 1 and 2, respectively. To understand further the nature of the phase transition, we plot order parameter probability distribution function (PDF) $P(\psi)$ vs. ψ in Fig.4.1(c) at the critical noise $\eta_c(\varepsilon) = 0.625,$ 0.640 and 0.654 for three $\varepsilon = 0,$ 1 and 2, respectively. For $\varepsilon = 0,$ there is a clear bimodal nature of $P(\psi)$ which gradually changes to unimodal on increasing

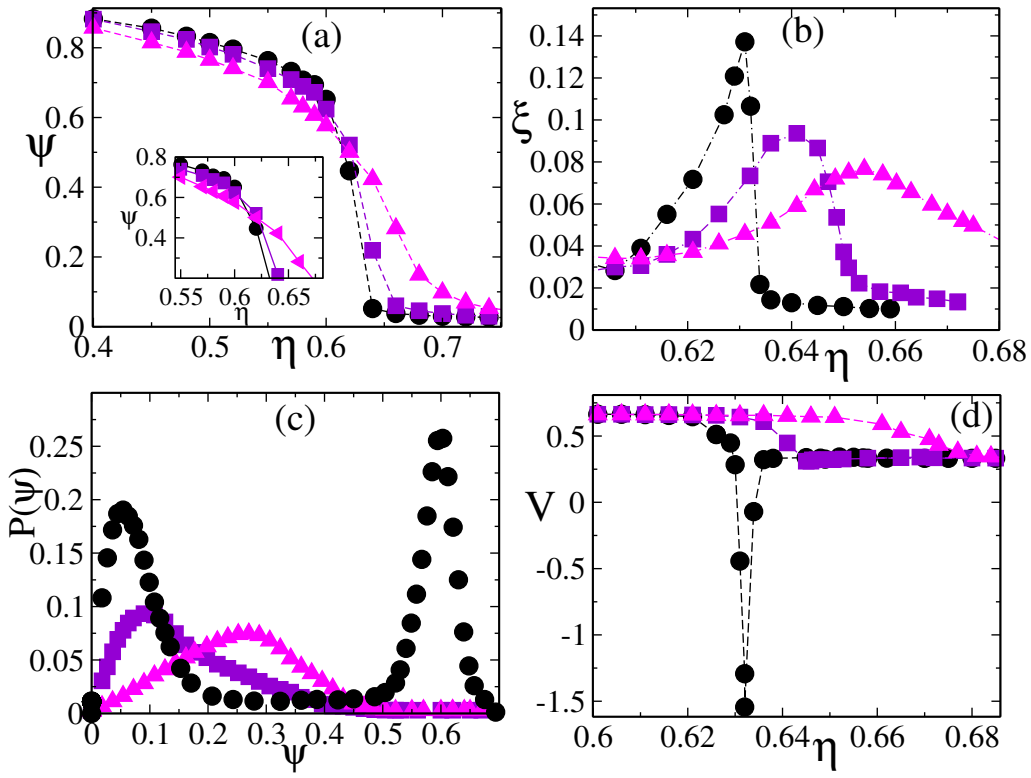

Fig. 4.1 (color online) (a) The plot of the mean orientation order parameter ψ *vs.* noise strength η, *inset*: zoomed plot shows enhanced ordering on increasing ε. (b) Variation of susceptibility ξ *vs.* ε. (c) The probability distribution function of order parameter $P(\psi)$ *vs.* ψ at the transition point ($\eta_c(\varepsilon)$ = 0.625, 0.640, and 0.654 for $\varepsilon = 0$, 1 and 2, respectively. (d) Variation of fourth-order Binder cumulant V *vs.* η. Different symbols imply different values of disorder strength $\varepsilon = 0(\circ)$, $1.0(\square)$, $2.0(\triangle)$ for the system size L=150 and the density $\rho_N = 1.0$.

ε. To characterise further, the nature of the transition for $\varepsilon = (0,\ 1$ and $2)$ in Fig.4.1(d), we calculate the fourth-order cumulant or the Binder cumulant $V = 1 - \frac{<\psi^4>}{3<\psi^2>^2}$ vs. η. We plot $V(\eta)$ vs. η in Fig.4.1(d). It shows strong discontinuity between $V = 1/3$ (for disordered state) to $V = 2/3$ (for ordered state) as we approach critical η_c for $\varepsilon = 0$. However, it goes smoothly between a disordered state $(V = 1/3)$ to an ordered state $(V = 2/3)$ for $\varepsilon = 2$.

***Finite-size analysis*:**- To characterise further, the nature of the phase transition more precisely, we perform the finite-size analysis of the system for different strengths of disorder ε. First, we plot the global orientation order parameter ψ vs. noise strength η for three disorder strengths $\varepsilon = 0$, 1 and 2 in Fig.4.2 (a)-(c), for four system sizes $L = 90$, 120, 150

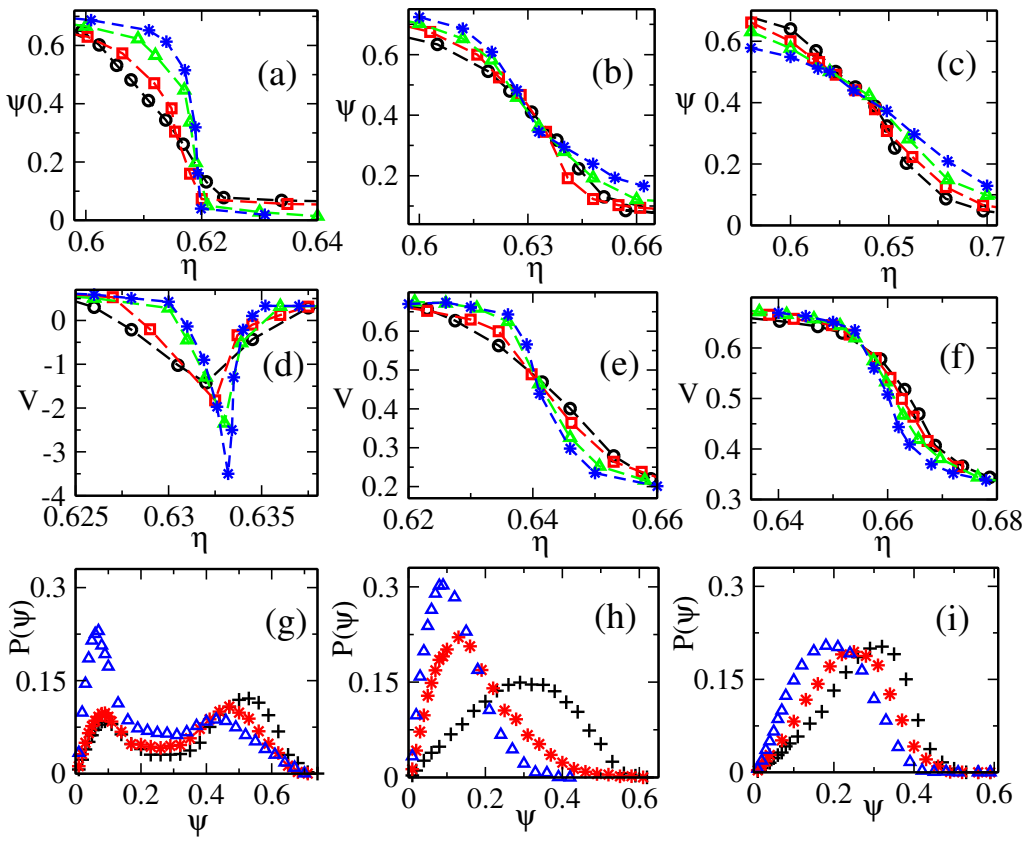

Fig. 4.2 (color online) Plot (a)-(c) show orientation order parameter ψ vs. η and (d-f) represent Binder cumulant V *vs.* η for $\varepsilon = 0$, 1 and 2. In plots (a)-(f) the black $\circ$, red $\square$, green $\triangle$ and blue $\star$ are for system sizes $L = 90$, 120, 150 and 200, respectively. (g)-(i) are plots of orientation order parameter distribution $P(\psi)$ keeping system size $L = 120$ for three different η values. (g) for $\varepsilon = 0$, $\eta = 0.6245$, 0.6260 and 0.6275, (h) $\varepsilon = 1$, $\eta = 0.6375$, 0.6390 and 0.6420, and (i) $\varepsilon = 2$ for $\eta = 0.6490$, 0.6520 and 0.6540, respectively. Symbols with color black '+', red '$\star$' and blue '$\triangle$' show the increase in η values with their respective ε values. In all the cases system density is fixed $\rho_N = 1.0$.

and 200, respectively. In Fig.4.2(a) for $\varepsilon = 0$, with the increase in the system size, clearly, the value of order parameter ψ, becomes more discontinuous on increasing system size. In Fig.4.2(b) for $\varepsilon = 1$, ψ becomes more continuous on increasing system size. For $\varepsilon = 2$ as shown in Fig.4.2(c), the ψ curves become more continuous on increasing system size compared to former ε values. Moreover, to further understand the effect of finite size on the phase transition, we calculate fourth-order Binder cumulant V for $\varepsilon = 0$, 1 and 2 in Fig.4.2(d)-(f) for four system sizes $L = 90, 120$, 150 and 200. For $\varepsilon = 0$ in Fig.4.2(d), with

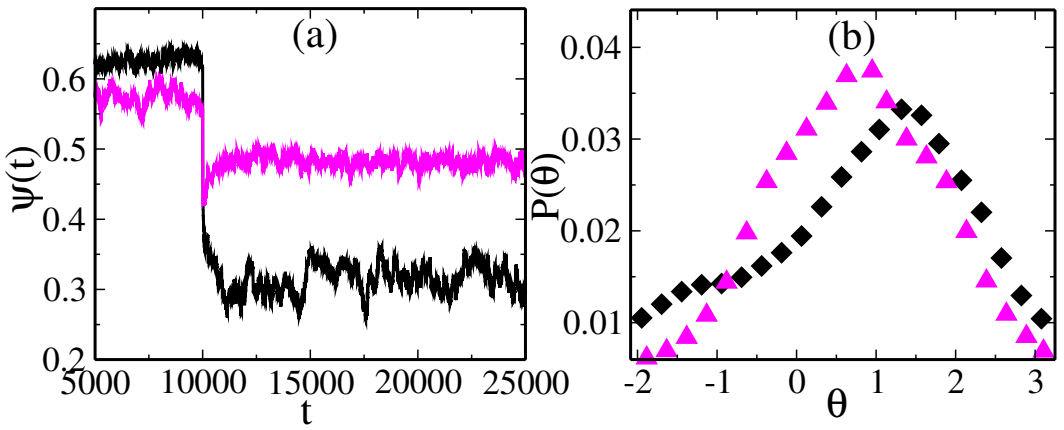

Fig. 4.3 (color online) (a) Time series of $\psi(t)$ for disorder $\varepsilon = 1.0$ (black line) and $\varepsilon = 2.0$ (magenta line). The two types of quenched impurities with orientations $\pm\frac{\pi}{2}$ are introduced at time $t = 10,000$. (b) PDF for the orieantation distribution $P(\theta)$ *vs.* mean orieantation θ, for $\varepsilon = 1.0$ ($\square$) and $\varepsilon = 2.0$ ($\triangle$). All the plots are for system size $L = 100$, noise strength $\eta = 0.62$ and the density $\rho_N = 1.0$.

the increase in the system size, V changes sharply, showing discontinuous phase transition. While for $\varepsilon = 1$ in Fig.4.2(e), V shows a smooth crossover. Further, in Fig.4.2(f) for $\varepsilon = 2$, we get a clear crossing of V at a single point with respect to different system sizes. This is one of the clear signatures of continuous transition. Finally, we calculate the orientation order parameter probability distribution function (PDF) $P(\psi)$ for $\varepsilon = 0$, 1 and 2 in Fig. 4.2(g)-(i), keeping system size 120 for three different η's. In Fig.4.2(g), for $\varepsilon = 0$, there is a clear bimodal signature for three $\eta = 0.6245$, 0.6260 and 0.6275. In Fig.4.2(h) for $\varepsilon = 1$ for three $\eta = 0.6375$, 0.6390 and 0.6420. Here we again find unimodal nature, but with a large tail. Further, in Fig.4.2(i) for $\varepsilon = 2$, $P(\psi)$ for three $\eta = 0.6490$, 0.6520 and 0.6540. Here it is very clear that $P(\psi)$ shifts towards the left slowly (continuous manner) with increased η, which confirms there is a clear continuous nature of the phase transition. Hence the above finite-size analysis and behaviour of PDF near critical point suggest the change in the nature of the phase transition from discontinuous type to the continuous type on the increasing strength of disorder ε. Further, we characterise the enhanced ordering near to the critical values of η and shift of $\eta_c(\varepsilon)$ towards higher values for $\varepsilon = 0$, 1 and 2 as shown in the inset of Fig.4.1 (a).

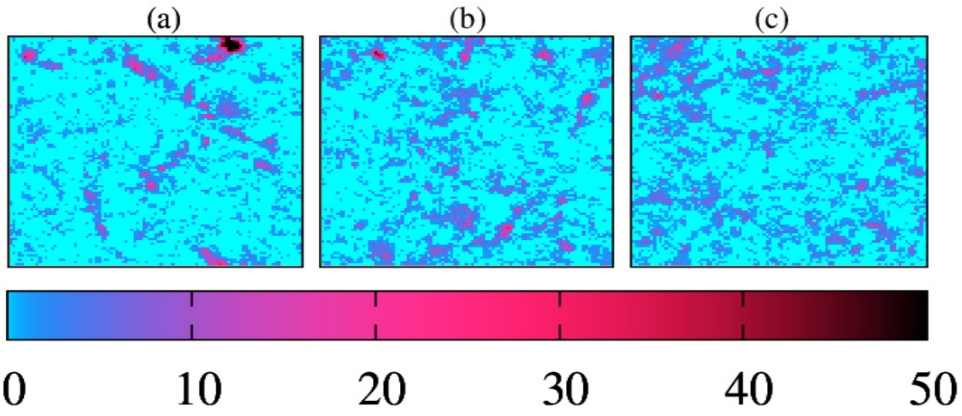

Fig. 4.4 (color online) Plot (a), (b) and (c) are the real space snapshots for three $\varepsilon = 0$, 1 and 2, respectively. The color bar shows the number of particles in the subshells. All the parameters are the same as in Fig.4.3.

Enhanced ordering :- To understand the enhanced ordering mechanism, we perform a small perturbative study on the system. Since we find enhanced ordering near $\eta \sim 0.6$, the perturbation is imposed at $\eta = 0.62$ for finite disorder $\varepsilon = 1$ and 2.

In the perturbative study, the system is awaited to reach the steady-state ($t = 10^4$) and once the steady-state is reached; we randomly choose 5% of the particles and out of which the direction of 2.5% particles with $J > 1$ quench to the direction $\frac{\pi}{2}$ and remaining 2.5% with $J < 1$ are quenched to the direction $\frac{-\pi}{2}$. Once this perturbation is applied, the system will respond to it and mean order parameter $\psi(t)$ shows a dip and then relaxes to a new steady-state with a relatively lower value of $\psi(t)$ as shown in Fig.4.3(a). Very clearly, before perturbation, ψ is lower for $\varepsilon = 2$, hence a more ordered state for the lower disorder. But after perturbation, which is selectively for particles with higher and lower J values, the response is different for $\varepsilon = 1$ and 2. For $\varepsilon = 2$, after perturbation ψ is larger compared to $\varepsilon = 1$. Hence more ordered state for the larger disorder. In the plot of Fig.4.3(b), we plot the orientation probability distribution function (PDF) $P(\theta)$ of the orientation of the particles θ. For $\varepsilon = 1$, the $P(\theta)$ shows two distinct peaks for $\theta = \pm\pi/2$, but the peak for $\pi/2$ or response to higher J is more. For $\varepsilon = 2$, the mean of the $P(\theta)$ shifts towards the non-zero θ, hence the system's response happens globally, and the whole system is

polarised in the direction of quenched particles with larger J values.

Now, we further study the consequence of such enhanced ordering for larger disorder on the polar flock. Moreover, this dominated alignment is responsible for the shifting of transition point η_c towards higher values.

4.3.2 Properties of the polar flock

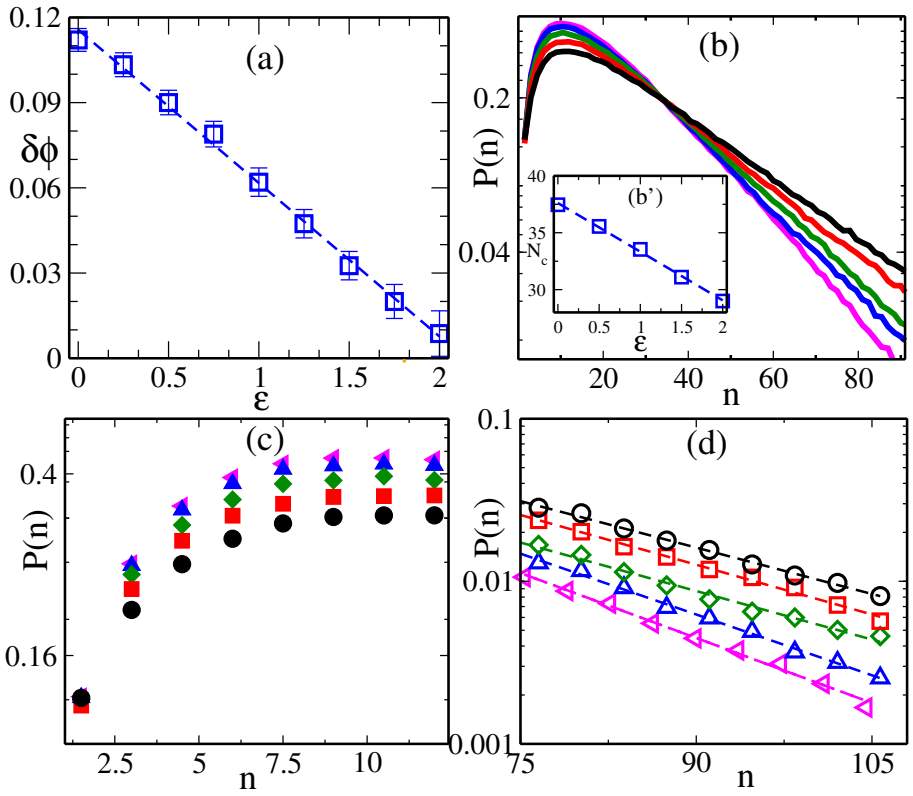

Fig. 4.5 (color online) (a) Plot of density phase separation order parameter $\delta\phi$ vs. ε with blue squares. The blue dotted line shows the linear decay of $\delta\phi$. (b) P(n) vs. n for $\varepsilon = 0$, 0.5, 1, 1.5 and 2. Different colors with lines black, red, green, blue and magenta are for $\varepsilon = 0$, 0.5, 1.0, 1.5 and 2.0. The inset of Fig.(b) shows the mean number of particles N_c vs. ε where the blue dotted line shows linear decay of N_c. (c) and (d) show the zoom plot of (b) near to the head and tail where the tail parts are fitted with exponential function with dotted lines. Symbols with black (circles), red (squares), green (diamonds), blue(triangles up) and magenta (triangles left) colors are for $\varepsilon = 0$, 0.5, 1.0, 1.5 and 2.0 in (c) and (d). Also, (b), (c) and (d) are in semi-log y-axis. All the parameters are the same as in Fig.4.3.

How does disorder affect the density fluctuations in the system? We plot real space snapshots of the local density (calculated in a small region of unit size square sub-shell) in Fig.4.4(a)-(c) for three values of $\varepsilon = (0,\ 1$ and $2)$ at time $t = 10^6$. For clean polar flock ($\varepsilon = 0$), particles form isolated clusters. Whereas with a non-zero ε, these isolated clusters break, and the system gets into a more homogeneous state. To further confirm this, we calculate the density phase separation order parameter, $\delta\phi$ vs. ε (where $\delta\phi(\varepsilon)$ is the deviation of the number of particles among the sub-cells), as shown in Fig.4.5(a). We calculate $\delta\phi$ by dividing the whole $L \times L$ system into unit sized sub-cells, $\delta\phi(\varepsilon) = \sqrt{\frac{1}{L^2}\sum_{j=1}^{L^2}(\phi_j(\varepsilon))^2 - (\frac{1}{L^2}\sum_{j=1}^{L^2}\phi_j(\varepsilon))^2}$ where ϕ_j is the number of particles in the j^{th} sub-cell and $\langle....\rangle$ represents averaging over 20 realisations. We note that $\delta\phi$ decreases in a linear fashion with increasing ε as shown in Fig. 4.5(a). Hence system becomes more homogeneous with increasing the random bond disorder ε in the system. Furthermore, in Fig.4.5(b), we plot the probability distribution function (PDF) of a number of neighbours $P(n)$ for different values of $\varepsilon = 0$, 0.5, 1, 1.5 and 2, respectively. Sharper tail for large n for the higher value of $\varepsilon = 2$ shows that the system is approaching towards a more homogeneous state or clusters of smaller size while the longer tail, for lower values of $\varepsilon = 0$, hence bigger clusters. In the inset of Fig.4.5(b), we plot the mean number of particles N_c with ε where N_c is obtained by fitting the tail of the main plot by the exponential function $\exp(\frac{-n}{N_c})$. This shows that N_c decreases linearly with an increase in the value of ε. Similarly, when zoomed for smaller n as shown in Fig.4.5(c), $P(n)$ for larger ε is higher as compared to smaller ε. Hence formation of small clusters have more probability for the larger disorder. Fig.4.5(d) shows the zoomed tail of the $P(n)$.

4.3.3 Accelerated response to external perturbation

We claim that enhanced ordering near-critical regions, and homogeneous density clusters promote faster response among the flock. To confirm the same, we perform another

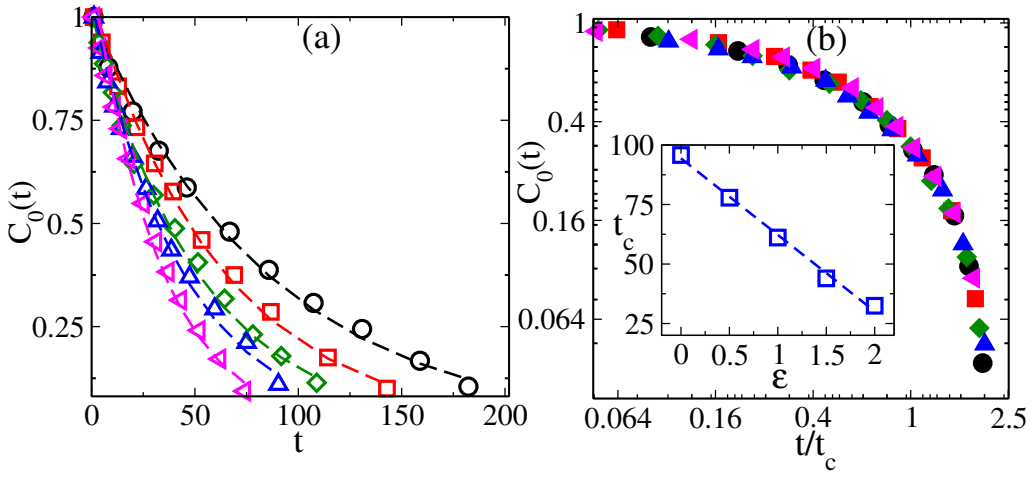

Fig. 4.6 (color online) (a) Plot of OACF $C_0(r,t)$ *vs.* t. for $\varepsilon = 0.0$ (circles), 0.5 (squares), 1.0 (diamonds), 1.5 (triangles up) and 2.0 (triangles left). Dashed lines are fit to exponential to the data (symbols). (b) Plot for $C_0(r,t)$ *vs.* scaled time t/t_c; and t_c *vs.* ε (inset) where the dashed lines are a linear fit to the data. All other parameters are the same as in Fig. 4.3

perturbation to the well-ordered flock in the steady-state and calculate its response. We randomly select a fraction of particles 1% and quench their direction to a randomly selected fixed orientation. With time all other particles will rotate in that direction. Their response to the direction of quench is measured by calculating the orientation auto-correlation function (OACF) $C_0(t) = \langle \cos\theta_i(t) - \theta_i(0)\rangle - \langle \cos\theta_i(T) - \theta_i(0)\rangle$. Where $\theta_i(t)$ and $\theta_i(0)$ are the orientation of the i^{th} particle at time t and 0 from the time of quench, and T is the late time when approximately all the particles are oriented in the direction of the quench. $\langle ....\rangle$ denotes averaging over all the SPPs over 30 independent realizations. In Fig.4.6(a), OACF $C_0(t)$ decays exponentially and shows the sharper decay with the increase in the strength of disorder ε. Therefore, the response of the flock to external perturbation becomes faster with the increase in ε. In Fig.4.6(b), we plot the $C_0(t)$ *vs.* scaled time t/t_c, where t_c is obtained from the fitting of $C_0(t)$ to $\exp(-t/t_c)$. The inset of Fig.4.6(b) shows the variation of t_c vs. ε. t_c shows linear decay with ε, which confirms the faster response of the flock towards external perturbation with an increase in the value of ε.

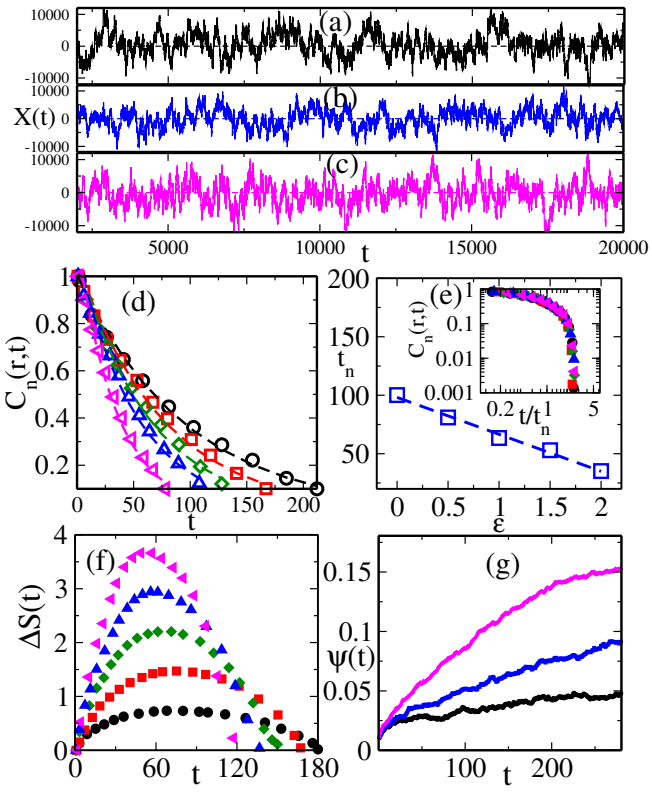

Fig. 4.7 (color online) (a), (b) and (c) show the variation of $X(t)$ *vs.* t. Black, blue and magenta colors are for $\varepsilon = 0$, 1 and 2, respectively. (d) Variation of neighbour fluctuation autocorrelation $C_n(r,t)$ *vs.* t. Symbols with black (circles), red (squares), green (diamonds), blue (triangles up) and magenta (triangles left) colors are for $\varepsilon = 0$, 0.5, 1.0, 1.5 and 2.0, respectively. Dashed lines are fit to exponential. (e) The plot of t_n vs. ε shows linear decay with ε; inset; the plot of correlation $C_n(r,t)$ *vs.* scaled time t/t_n. (f) The plot of the systems' information entropy ΔS(t) *vs.* t. (g) Time evolution of $\psi(t)$ with time t where colors black, blue and magenta are for $\varepsilon = 0$, 1 and 2, respectively. All other parameters are the same as in Fig. 4.3

4.3.4 Disorder increases the systems' information entropy

Further, we claim that the accelerated response to external perturbation is due to neighbours' frequent updates for high disorder strength.

We define the update in the neighbour list of the SPPs as $X(t) = \frac{1}{N}\sum_{i=1}^{N}((< N_R^i(t) \times N/2 >) - \sum_{j\in R} j)$. Where N_R^i is the number of SPPs inside the interaction radius of the i^{th} particle, N is the total number of particles in the system and the second term on the right-hand side is the sum over all the particle indices j inside the interaction radius of the i^{th} particle. The

time series of $X(t)$ oscillates around 0 for different values of ε, as shown in Fig.4.7(a), (b) and (c). The frequency of oscillation of $X(t)$ increases with increasing ε. The increase in the oscillation frequency of $X(t)$ suggests more frequent updates of the neighbour list and the decrease in the magnitude of $X(t)$ implies a lesser number of neighbours inside the interaction radius of an SPP. Furthermore, we calculate the neighbour autocorrelation function,

$$C_n(t) = \Big\langle \frac{\sum_{t'=1}^{T-t}(X(t')-\overline{X})(X(t'+t)-\overline{X})}{\sum_{t'=1}^{T}(X(t')-\overline{X})^2} \Big\rangle \tag{4.4}$$

where $\overline{X}$ is the mean value of $X(t)$ over the total time T and $t < T$. $\langle ....\rangle$ represents averaging over 20 independent realisations. In Fig.4.7(d), faster decay of $C_n(t)$ with increase in the disorder strength ε, suggests more frequent update of neighour list. Also, in the inset of Fig.4.7(e), we plot the scaled correlation $C_n(t)$ vs. t/t_n where t_n is obtained by fitting the exponential function to $\exp(\frac{-t}{t_n})$. In Fig.4.7(e), we have shown the variation of t_n with ε which decays linearly. Now we use the systems' information entropy [Ben-Naim (2015); Cavagna et al. (2014)] approach to show that the larger the disorder, the larger is the systems' information entropy and hence the more information transfer among the SPPs. The faster information transfer in more disorder system is due to the possibility of more number of accessible states for the particles. Each state can be defined as the new neighbour in the chosen particle's contact list, if we denote P_s, as the probability of being in the i^{th} states from the set of all possible accessible states. If a particle changes its neighbours frequently, it is exploring more number of neighbouring particles and hence more number of states. Hence the neighbour autocorrelation, $C_{n,s}(t)$, (the quantity inside the $< ... >$ of Eq $\sim$(4.4) is the neighbour autocorrelation for one state. The subscript s denotes the different independent configurations and hence different sets can be generalised as different independent configurations. And $C_{n,s}(t)$ and $P_s(t)$ are equivalent. One is the measure of the probability of being in a given neighbour list, and is the same as $P_s(t)$. As time progresses $C_{n,s}(t)$ decreases, and hence more and more states are accessed. Hence we

define the systems' information entropy of the system as $\Delta S(t) = -\sum_s C_{n,s}(t) \ln_2 C_{n,s}(t)$, where summation s is over all possible realisations. Larger the systems' information entropy, larger the available microstate for the particles, and hence the more information transfer among the flocks. We plot the variation of the systems' information entropy $\Delta S(t)$

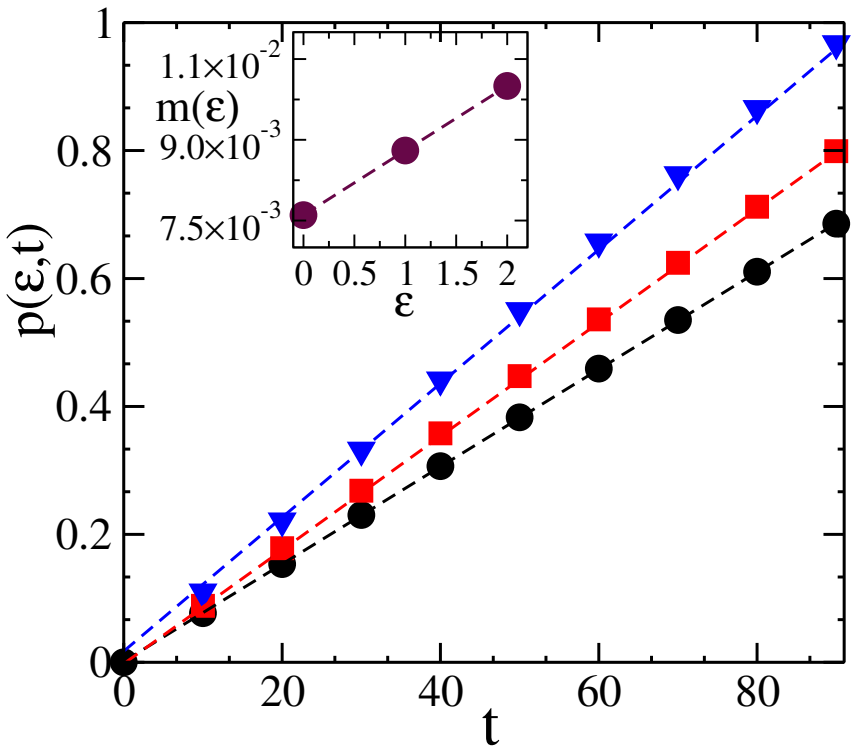

Fig. 4.8 (color online) The plot shows the probability of newly visited particles $p(\varepsilon,t)$ with respect to time t for three values of ε. Black $\circ$, red $\square$, and blue $\triangle$ are for $\varepsilon = 0$, 1 and 2, respectively. Color dotted lines show the data fit with fitting function $p(\varepsilon,t) = m(\varepsilon) \cdot t$ where $m(\varepsilon)$ is the slope. In the inset, we show the m vs. ε which increases linearly. Other parameters are the same as in Fig.4.3

for different disorders in Fig.4.7(f). We note that $\Delta S(t)$ increases with ε which further confirms that particles are exploring more states for higher disorder strength hence more information transfer. Also, in Fig.4.7(g), we have plotted the time evolution of order parameter in the early time, which shows that for larger ε, the system reaches the ordered state quicker in comparison to the lower ε. Further, we also show the quicker update of the neighbour list for a single particle. In Fig.4.8 , we plot the fraction of new particles $p(\varepsilon,t)$

in the neighbour list of a given particle from some reference time $t_0 = 0$. At time t_0, all the particles are labeled as old, hence $p = 0$. Time in Fig.4.8 , is measured from the reference time t_0, hence reference time is time zero on the $x-$axis. As time progresses, new particles come in the contact list of the given particle, and $p(\varepsilon,t)$ starts to increase. At a very late time, all the old particles are gone out of the neighbour list, and hence $p = 1$. As shown in the figure, for the larger disorders, new neighbours are updated faster than for the small disorder. In the inset of Fig.4.8 , we show the linear increase of slope $m(\varepsilon)$ with respect to $\varepsilon = 0$, 1 and 2 where $m(\varepsilon)$ is obtained from fitting the main plot with the linear fitting function.

4.4 Discussion

We introduce a minimal model for a collection of self-propelled particles with bond disorder. Each particle has a different ability (interaction strength) to influence its neighbours. The varying interaction strength is obtained from a uniform distribution, and it can be varied from $[1-\varepsilon/2 : 1+\varepsilon/2]$, where ε is the disorder strength. For $\varepsilon = 0$, the model reduces to the constant interaction strength model or the Vicsek-like model [Vicsek et al. (1995)]. We have studied the steady-state characteristics for different strengths of the disorder near to order-disorder transition. To our surprise, bond disorder leads to faster information transfer within the flock viz; the systems' information entropy gets increased.

Our numerical study also shows that the disorder-to-order transition is discontinuous in the disorder-free system and changes to continuous type with an increase in disorder. Furthermore, the transition point shifts towards the higher η for the large disorder.

Our study provides a new direction to understand the effect of intrinsic inhomogeneity in many natural active systems. It shows how the bond-disorder in the system can enhance ordering, and faster information transfer among the particles. Such properties can be useful

for many applications: like the faster evacuation of active particles, and also for crowd control in many social gatherings.

****